THE JOURNAL OF PHYSICAL CHEMISTRY B

Article

pubs.acs.org/JPCB

Theoretical Study of Water Oxidation by the Ruthenium Blue Dimer. II. Proton Relay Chain Mechanism for the Step $[bpy_2(HOO)Ru^{IV}ORu^{IV}(OH)bpy_2]^{4+} \rightarrow [bpy_2(O_2^-)Ru^{IV}ORu^{III}(OH_2)bpy_2]^{4+}$

Roberto Bianco,*[,†] P. Jeffrey Hay,[†] and James T. Hynes[†,‡]

[†]Department of Chemistry and Biochemistry, University of Colorado, Boulder, Colorado 80309-0215, United States

[‡]Chemistry Department, Ecole Normale Supérieure, UMR ENS-CNRS-UPMC 8640, 24 rue Lhomond, 75005 Paris, France

Supporting Information

ABSTRACT: The oxidation of water to O_2 by the oxidized species $[L_2(O)Ru^{V}ORu^{V}(O)L_2]^{4+}$ of the Ru blue dimer catalyst (L = bpy, bipyridine) is examined using density functional theory with model ligands and explicit solvent approaches. Following our earlier study of the initial O−O formation by addition of water (step I) (*J. Phys. Chem. A* **2011**, *115*, 8003), we report calculations on the subsequent, penultimate step in the superoxide production (denoted step II), involving proton transfer from the reactant $[L_2(HOO)Ru^{IV}ORu^{IV}(OH)L_2]^{4+}$ to form $[L(O_2^-)Ru^{IV}ORu^{III}(H_2O)L_2]^{4+}$. The reaction profile of step II commences with a rearrangement of the HOO and OH groups and associated solvent relaxation in the complex, accompanied by a barrier of ∼9 kcal/mol and a free-energy change of +3 kcal/mol. Subsequently, a water molecule connecting these two groups mediates a double proton transfer in a proton relay chain that proceeds spontaneously with a free-energy decrease of 8 kcal/mol to form step II's product. Comparison with other calculations is made, and the implications for the overall water oxidation to O_2 are discussed.

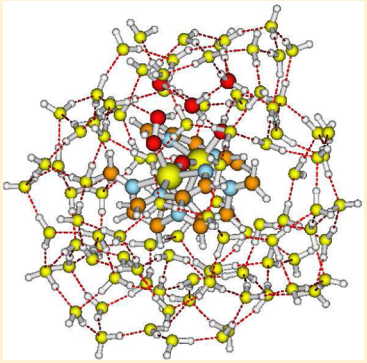

1. INTRODUCTION

The prospect of developing inorganic catalysts for water oxidation

$$2H_2O \rightarrow O_2 + 4H^+ + 4e^- \quad (1)$$

for hydrogen and oxygen generation using solar energy has become an increasingly active area as new types of complexes have been found[1−19] that mimic the natural water oxidation catalytic system in the oxygen-evolving complex of photosystem II in plants.[7]

In parallel to these experimental efforts, theoretical studies have sought to understand the basic steps in assorted water oxidation systems using density functional theory and other approaches.[20−27] We have recently been examining one of the first discovered water-oxidizing catalysts, the well-known ruthenium blue dimer $[(bpy)_2(H_2O)Ru^{III}ORu^{III}(H_2O)(bpy)_2]^{4+}$,[8−11] where bpy denotes bipyridine. In particular, we examined[23] the initial step in the catalytic process identified by Meyer and co-workers involving the oxidized form of the dimer

$$[(bpy)_2(O)Ru^{V}ORu^{V}(O)(bpy)_2]^{4+} + H_2O \rightarrow [(bpy)_2(HOO)Ru^{IV}ORu^{IV}(OH)(bpy)_2]^{4+} \quad (2)$$

As shown in the mechanism in Figure 1, in our view, the reaction involves an additional H_2O molecule to carry out the proton transfer (PT) between the ligands on each end of the Ru dimer. In the current paper, we focus on the subsequent step, in which a proton is transferred from the RuOOH group to the RuOH group

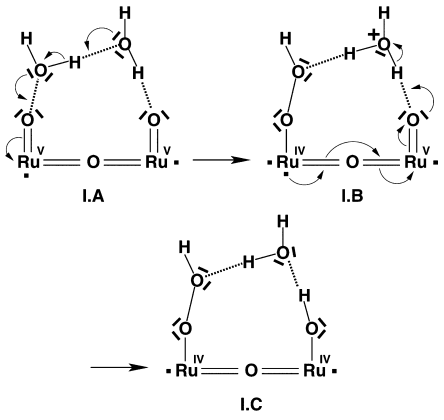

Figure 1. Mechanistic scheme for the O−O bond formation step (step I in the mechanism herein) of water oxidation by $[(bpy)_2(O)Ru(V)-O-Ru(V)(O)(bpy)_2]^{4+}$ shown as I.A in the figure and denoted in water oxidation by $[O(V,V)O]^{4+}$ in the text. In the proton relay mechanism, the attacking H_2O forms the O−O bond, and the second H_2O affects PT to the opposite end of the dimer.

Special Issue: Michael D. Fayer Festschrift

Received: July 1, 2013
Revised: August 14, 2013
Published: August 16, 2013

dx.doi.org/10.1021/jp406504h | *J. Phys. Chem. B* 2013, 117, 15761−15773

$$[(bpy)_2(HOO)Ru^{IV}ORu^{IV}(OH)(bpy)_2]^{4+} \rightarrow [(bpy)_2(O_2^-)Ru^{IV}ORu^{III}(H_2O)(bpy)_2]^{4+} \quad (3)$$

leaving a superoxide ion on the original Ru center. This PT step in eq 3 forms the central focus of the present paper and will be denoted as step II; we refer to the previous step eq 2 as step I.[28] For convenience, we adopt here the concise notation $[XmnY]^{4+} \equiv [(bpy)_2(X)Ru^mORu^n(Y)(bpy)_2]^{4+}$, where m, n = III, IV, V oxidation states and X, Y denote ligands O (for O^{2-}), OOH (for OOH^-), OH (for OH^-), O_2, and H_2O. The step II reaction in eq 3, for example, will be written $[HOO(IV,IV)\text{-}OH]^{4+} \rightarrow [O_2^-(IV,III)H_2O]^{4+}$ in subsequent sections.

The superoxide ion in the penultimate complex $[O_2^-(IV,III)\text{-}H_2O]^{4+}$ in eq 3 must be evolved in a dissociation to produce the free dioxygen molecule in a subsequent step

$$[O_2^-(IV, III)H_2O]^{4+} + H_2O \rightarrow [H_2O(III, III)H_2O]^{4+} + O_2 \quad (4)$$

The step II reaction in eq 3 is not rate-determining in the overall water oxidation; the step I reaction in eq 2 plays that key role,[23] but it is important in producing the penultimate complex $[O_2^-(IV,III)H_2O]^{4+}$ involving the superoxide ion in the ultimate step in eq 4.

It is important for the present work to note that our perspective for the O−O single bond formation step I, depicted in Figure 1, involves an initial nucleophilic attack on an oxo O by a water molecule (I.A) coupled to PT in a proton relay chain (PRC) involving two waters in the chain. In the PRC, two successive PTs occur, a PT from this water to the H-bonded solvent water (I.B) and then a second PT to the other Ru═O group.

Just as we found[23] a PRC route for step I, we argue within that another PRC route is involved in step II (eq 3) in transferring a proton from the left-hand side OOH moiety in the $[HOO(IV,IV)OH]^{4+}$ reactant complex (RC) to ultimately protonate the OH moiety on the right-hand side of the complex to produce an incorporated water molecule. Inspection of the product complex (PC) in Figure 1 for our step I mechanism suggests, and we will find, that a single water molecule forms the keystone of the PRC for step II.

The outline of the remainder of this paper is as follows. Section 2 is devoted to a detailed discussion of the mechanistic hypothesis for the step II reaction. The computational procedure is presented in section 3, including discussion of the quantum chemical calculations and the inclusion of aqueous solvent effects. The reaction path for step II is presented and analyzed in section 4. The rearrangement process needed to prepare the product from step I for the PRC reaction is described in section 5. A reaction scheme for water oxidation comprising the present step II and the preceding step I is discussed in section 6. Comparisons with previous calculations are presented in section 7, and concluding remarks are offered in section 8.

2. MECHANISTIC HYPOTHESIS

In analogy to our procedure in our previous effort[23] on step I of the water oxidation by the blue dimer, here we initially construct a mechanistic hypothesis for the reaction step II. As indicated in the Introduction, we anticipate that a PRC mechanism is involved, here depicted in Figure 2, which displays the transition-metal (TM) complex and a PRC water molecule that is H-bonded to both the −OOH and −OH

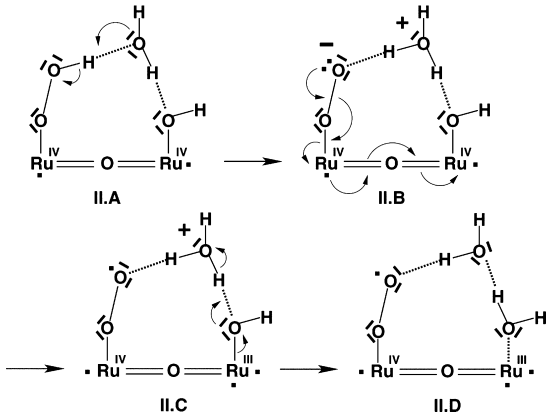

Figure 2. Mechanistic hypothesis for the proton relay of step II in the water oxidation scheme where $[HOO(IV,IV)OH]^{4+}$ (II.A) is converted to $[O_2^-(IV,III)H_2O]^{4+}$ (II.D). The $Ru-O_2^{\bullet}$ bond in II.D is ionic, with a negative charge formally assigned to the O_2 moiety, which is therefore to be intended as a superoxide ion O_2^- here and elsewhere in the text. Neither the organic ligands nor the solvent molecules are shown.

groups of the complex, that is, Ru−OOH···O(H)H···O(H)−Ru. Other spectator waters, whose H-bonding interactions with the complex help shape the potential energy surface (PES) for the PT reaction, have been omitted from the figure; we will discuss their role below.

Consideration of the charge flows highlighted in Figure 2, which lead to the intermediates and products of the reaction, guide our choice of the model reaction system, which we will later construct in order to examine step II. The sequence of PT and electron transfer (ET) events in this hypothesis is chosen in order to highlight their causality and synergism. This sequence might not be exactly realized in the details of the calculated reaction path, where charge flows involve fractional electronic charges rather than the full charges employed in Figure 2; nonetheless, our procedure proves to be a powerful tool in anticipating the important features of the reaction.

There is an important point to make concerning the mechanism in Figure 2. The conformation of the TM complex resulting from step I (see the product I.C in Figure 1) is *not* that appropriate for PT from Ru−OOH to Ru−OH. The appropriate conformation is depicted in Figure 2, structure II.A. The conversion from the former structure to the latter (Figure 3), which involves several H-bond rearrangements, must be

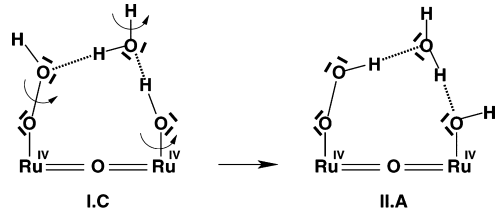

Figure 3. Required conformational change in the product (I.C) of O−O bond formation in step I to obtain the RC (II.A) in step II.

included in the reactive process that we henceforth term step II (Figure 2) in order to represent the reaction in eq 3. In contrast to step II (Figure 2), the rearrangement Figure 3 does not involve any breaking or making of chemical bonds and should not prove costly in energy. Accordingly, we here simply commence the mechanistic hypothesis discussion assuming that

dx.doi.org/10.1021/jp406504h | J. Phys. Chem. B 2013, 117, 15761−15773

structure II.A is the relevant RC. The analysis of the conversion Figure 3 is presented in section 5.

2.1. II.A → II.B. In this initial portion of our proposed mechanism, the Ru−OOH group transfers a proton to the water molecule in the PRC. This PT is promoted by specific variations in H-bonding occurring at both the donor peroxydic group H-bearing O and the H_2O acceptor. In particular, the acidity of −OOH can be enhanced by stronger H-bonding to both lone pairs on the H-bearing O, while the basicity of the acceptor H_2O oxygen can be enhanced by (i) decreased H-bonding to the uncoordinated O lone pair and (ii) increased H-bonding to the water hydrogens by the Ru−OH oxygen and the oxygen of a solvent water (not shown).

The PT-promoting H-bonding to −OOH also stabilizes the ensuing $-OO^-$ peroxy anion, which supports the relevance of resonance structure II.B. Note that in this step, the charge of the TM complex decreases from 4+ to 3+. The presence of the hydronium ion in II.B has several implications from the point of view of the consideration of solvation effects, which are not explicitly dealt with in the scheme (but will be in the discussion of the calculation results). In particular, the surrounding H-bonding network has to create not only the conditions for PT from Ru−OOH to H_2O to occur but also those for ensuring that H_3O^+ is stabilized to some degree and, eventually, can transfer a proton to the hydroxo group Ru−OH.

2.2. II.B → II.C. In this mechanistic portion, electronic charge flows from $-OO^-$ across the μ-oxo bridge to the Ru−OH group. This ET across several bonds is key to the synergetic character of step II because it increases the electron density of the hydroxy proton acceptor on the right-hand side. It is promoted by (i) decreased H-bonding to $-OO^-$, ii) possibly an appropriate conformation of the O−Ru═O═Ru−O group favoring orbital overlap within the Ru═O═Ru unit, and (iii) increased H-bonding to the lone pairs of the hydroxy O, which makes this center more electrophilic. In view of the release of the O_2 molecule in its triplet state in step III (eq 4) of the water oxidation process, we depict the terminal O in Ru−OO with an unpaired electron.

2.3. II.C → II.D. Finally, there is PT from the hydronium ion to the right-hand side hydroxo. This PT is promoted by (i) decreased H-bonding to one or both of the other protons of the H_3O^+, destabilizing the cation; (ii) increased H-bonding to the H_3O^+ oxygen lone pair, with concurrent increase in the acidity of all of the H_3O^+ protons; (iii) increased H-bonding to the H of the Ru−OH unit, resulting in enhanced basicity of the oxygen; and (iv) shift of electron density from Ru to OH.

In the three mechanistic substeps just discussed, one aspect that we have not dealt with explicitly is the coordination number of the water (and its protonated hydronium form) at the center of the PRC. In particular, to avoid complicating the scheme, we have left out two spectator waters, one H-bonded to a lone pair and the other to a H of the central water. While neither of these two extra waters directly engages in ET or PT, the variation in their H-bonding to the central water can greatly affect the stability or lack thereof of the ensuing H_3O^+. We will highlight these aspects when we discuss the results of the calculations.

Within the framework of proton-coupled electron transfer (PCET),[29−32] our proposed mechanism can be classified as a solvent-assisted, multiple-site, electron−proton transfer (MS-EPT). Alternatively, although perhaps more prosaically, the mechanism is a double PT reaction in a PRC.

3. COMPUTATIONAL ASPECTS

The considerations of section 2 inform our modeling of the PT reaction system for step II in these calculations. The method employed is very similar to that in ref 23; therefore, we will be brief here.

The initial structure, designated as the core reaction system (CRS) and for which quantum chemistry is applied, comprises the $[L_2(HOO)Ru^{IV}ORu^{IV}(OH)L_2]^{4+}$ dimer and the PT-mediating water molecule shown in Figure 2 plus two additional water molecules. The additional water molecules are H-bonded to the H_2O's lone pair and the proton not coordinated to the Ru−OOH and Ru−OH groups, respectively, so as to provide proper solvation for the hydronium ion produced during the reaction.[33] The resulting $[L_2(HOO)Ru^{IV}ORu^{IV}(OH)L_2]^{4+}\cdot(H_2O)_3$ CRS is depicted in Figure 4. To make the calculations practical, the bpy ligands $(NC_5H_4)_2$ have been replaced by their smaller mimics L = $[CH_2{=}NC(H){=}]_2$; support for this replacement is provided in ref 23.

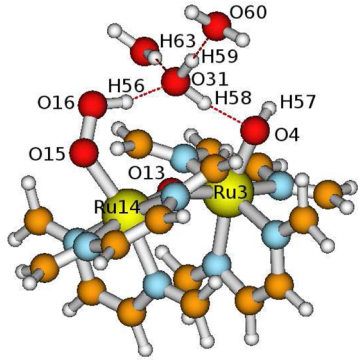

Figure 4. Labeling scheme for the $[HOO(IV,IV)OH]^{4+}\cdot(H_2O)_3$ CRS in which all atoms are treated quantum chemically. The starting RC structure is shown. H: white, O: red, N: blue, Ru: dark yellow, C: brown.

To construct the actual system used in the study of the reaction path, a partially optimized CRS is embedded within a lattice with the structure of hexagonal ice containing only the oxygen atoms.[34] The O−O distance in the lattice is set to 2.843 Å, derived from the $H_2O\cdot W_4$ cluster's optimization, where the central H_2O is described quantum chemically and W represents the classical, polarizable water of fixed internal structure r(OH) = 0.9438636 Å and a(HOH) = 106.70327°[35,36] used in the calculations. The target cluster size is obtained by retaining only the oxygens within a sphere of chosen radius centered on the μ-oxo oxygen of the $[HOO(IV,IV)OH]^{4+}$ species. Each oxygen in the lattice has four available positions, at the vertices of a tetrahedron, for the assignment of two hydrogens, thus yielding six possible orientations for the dipole moment of each water. The OH distance for the assignments of the H positions is set equal to 0.9438636 Å. The charges within the CRS, derived from a single-point calculation, are used in conjunction with the spherical cluster waters' dipole moments to calculate a charge-dipole interaction energy; this is minimized via a Monte Carlo algorithm, varying the orientations of the dipoles of all of the classical waters among the allowed orientations (six for each water). Finally, for each water, the HOH tetrahedral angle of ∼109.47°, used in the Monte Carlo algorithm to optimize H-bonding in the cluster, is decreased to 106.70327°, as required, by moving the hydrogens while preserving the OH bond

dx.doi.org/10.1021/jp406504h | J. Phys. Chem. B 2013, 117, 15761−15773

lengths and the dipole moment's direction. The resulting structure shows all of the classical waters H-bonded to the CRS and to each other. Subsequent optimization of the H-bonded assembly, with the CRS constrained, relaxed the position and orientation of the solvating waters, yielding the model reaction system (MRS) with an overall formula of $[HOO(IV,IV)OH]^{4+}\cdot(H_2O)_3\cdot W_{98}$, shown in Figure 5, for which reaction path calculations are performed.

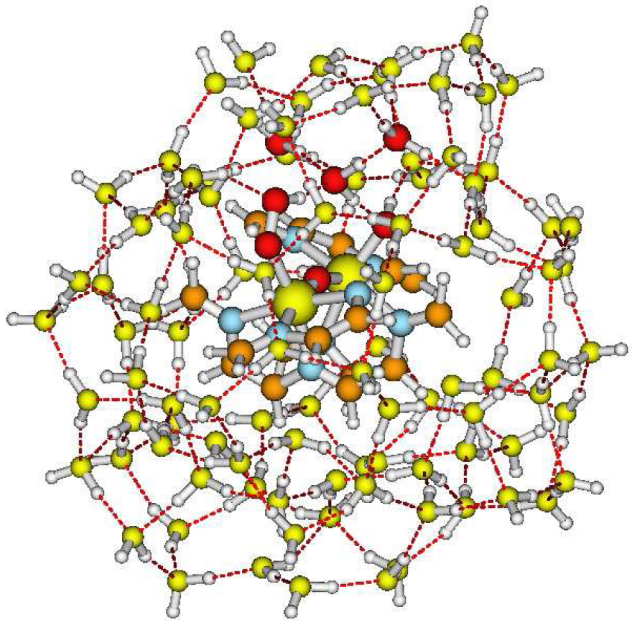

Figure 5. Structure of the $[HOO(IV,IV)OH]^{4+}\cdot(H_2O)_3\cdot W_{98}$ MRS used in the calculations, where the oxygens in the classical solvating waters are shown in yellow.

DFT/UHF/B3LYP calculations on the triplet electronic state of the $[HOO(IV,IV)OH]^{4+}\cdot(H_2O)_3\cdot W_{98}$ MRS were carried out with the exchange functional B88/HFX and the correlation functional LYP88/VWN5[37−41] on a Lebedev grid with 302 angular points and 96 radial points using GAMESS[42] with the valence-only, effective core potential SBKJC basis set for Ru and the SBKJC(d) basis set for all second-row atoms.[43,44] The choice of the triplet state is consistent with that justified in our previous paper on single O−O bond formation for the blue dimer.[23]

Additional calculations (section 5) with the system embedded in a dielectric continuum were performed with the PCM option in GAMESS with the default cavity radii for all of the atoms except for Ru, where the radius was chosen as 2 Å. A dielectric constant of 78.39 was used with a temperature of 298 K.

The molecular structures were drawn with Molden.[45] The mechanistic schemes were drawn with Xfig.[46]

4. PT REACTION PATH IN STEP II

In this section, we examine the pathway for PT in step II between the ends of the PC dimer PC(I) according to the reaction schematically denoted $[HOO(IV,IV)OH]^{4+} \rightarrow [O_2^-(IV,III)OH_2]^{4+}$ in our shorthand nomenclature. (Although we introduced this nomenclature in section 1 with the bpy ligands present in the complex, we will retain it in the remaining discussion for complexes with the replacement ligands, unless some confusion could arise.) The quantum chemically treated CRS is shown in Figure 4 with atomic labeling, while the fully solvated MRS with classical EFP waters is shown in Figure 5. The PT will be shown to be effected via an intervening H_2O species H-bonded to the dimer, as anticipated in the PRC mechanism in section 2. The nature of the RC for step II, RC(II), is discussed in section 4.1, and the detailed reaction with explicit solvation leading to formation of the PC(II) is given in section 4.2. That section addresses the calculated bond lengths, charges, and spins all along the reaction path. Section 4.3 discusses the evolving charge distributions in the context of aqueous solvent effects on the reaction barrier.

4.1. Examination of the RC. We first examine the RC for step II corresponding to structure II.A in the mechanistic hypothesis in Figure 2.

The unconstrained optimization of the initial MRS prepared according to the procedure described in section 3, instead of producing a relaxation to a minimum-energy structure, resulted in the spontaneous, sequential occurrence of both PTs in the PRC described in Figure 2. Because we were concerned that the PTs could be triggered by solvent configurations not equilibrated to the solute, we performed a constrained optimization of the initial MRS with the O16−H56 distance held fixed at its initial value of 1.0 Å in order to prevent the first PT. This procedure forces the classical waters solvating the CRS to equilibrate to an unreacting CRS structure, thus eliminating solvent configurations that could promote PT and biasing of the MRS toward stabilization into a PES minimum.

However, once the O16−H56 = 1.0 Å constraint was relaxed after a lengthy optimization, the full optimization again resulted in the two barrierless PTs and the generation via a PRC of the PC $[O_2^-(IV,III)OH_2]^{4+}$. This is a strong indication of the spontaneous character of step II once a PRC-compatible arrangement is formed among a water molecule and the Ru−OOH and Ru−OH groups in $[HOO(IV,IV)OH]^{4+}$. We now discuss the structural and electronic features along this optimization path.

Our results clearly indicate that once the PRC-compatible arrangement is in place, the two PTs are spontaneous. This suggests that our "RC" is in fact already past the transition state (TS) on the products' side. Therefore, the actual TS must involve motions leading to the *establishment* of the PRC. Because the starting, stable point is PC(I) for step I, we know that the nature of the motions leading to the TS must involve a conformational change in the whole complex, concerning primarily the Ru−OOH and Ru−OH groups, as illustrated by Figure 3. This is the prior rearrangement that we already noted in our section 2 discussion of our mechanistic hypothesis in connection with that figure. However, given the strong H-bonding of these two groups to the solvating water molecules, this conformational rearrangement has to involve several H-bonds being broken and re-formed in either a sequential or concerted fashion, or both, with the resulting structural perturbations spreading to the first and second solvation shells. It is likely that the structure of the TS for the rearrangement is similar to the structure of PC(I) because the reaction path for step II is exothermic. Once the PRC is formed, the two PTs proceed spontaneously. We will return to the rearrangement itself in section 5 but for now proceed with the detailed calculation of the reaction path for step II, commenting as appropriate on the similarities and differences with our mechanistic hypothesis in Figure 2.

dx.doi.org/10.1021/jp406504h | J. Phys. Chem. B 2013, 117, 15761−15773

4.2. Reaction Path with Explicit Solvation. In the ensuing discussion, we will make frequent reference to Figure 6,

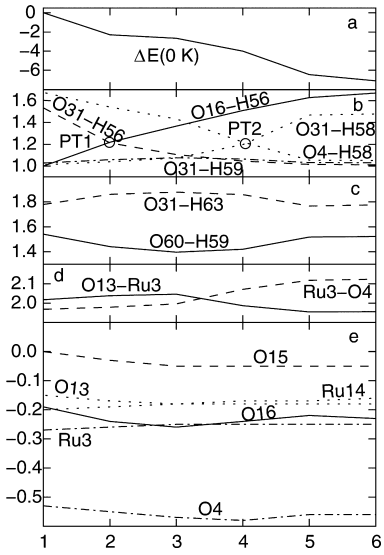

Figure 6. Computed properties along the reaction path during the PT stage of step II. The points 1−6 on the abscissa correspond to key structures along the optimization path, as shown in Figure 7. Panels from the top: (a) energy difference at 0 K (in kcal/mol) referenced to the reactant of step II, RC(II); (b) O−H bond lengths (in Å) for first (PT1) and second (PT2) PT events, marked by the small circles; (c) H-bonds O31−H63 and O60−H59 (in Å) to the water in the PRC; (d) O−Ru−O−Ru−O group bond lengths (in Å); and (e) Löwdin atomic charges (in au).

where the data displayed correspond to six selected structures along the optimization path referred to in section 4.1, namely, (1) an unstable RC, used as an energy reference; (2) PT1; (3) the intermediate region between the two PTs; (4) PT2; (5) the end of PT2; and (6) PC. The six selected structures are displayed in Figure 7. The atomic labeling scheme is displayed in Figure 4 and is also superimposed on the first structure of Figure 7.

While Figure 6 emphasizes trends of key features along the reaction path, more detailed data, to which we will refer as the need arises, are reported in several tables: (i) Table 1 for structural parameters of the PRC, (ii) Table 2 for structural parameters of the O−Ru═O═Ru−O group, (iii) Table 3 for the atomic $\alpha - \beta$ spin densities of the OO−Ru═O═Ru−O group, and iv) Table 4 for atomic charges.

We first note that the reaction at 0 K is exothermic by ∼7 kcal/mol (cf. Figure 6a). The monotonic, decreasing character of the six-point energy profile reflects that of the complete optimization profile (see the Supporting Information), which shows no intermediates. Because the RC is not a minimum on the PES, we could not use the vibrational frequencies of RC(II) to calculate the free energy of the reaction. Instead, we have embedded the RC(II) and PC(II) MRSs in a dielectric continuum of constant ε = 79.8 for water and obtained the free energy via single-point calculations. The resulting reaction free energy at 298 K is −7.9 kcal/mol, only slightly more negative than the 0 K reaction energy.

For the discussion of the reaction path, it is convenient to divide the latter into three regions, (i) before PT1, (ii) between PT1 and PT2, and (iii) after PT2, with PT1 and PT2 marked

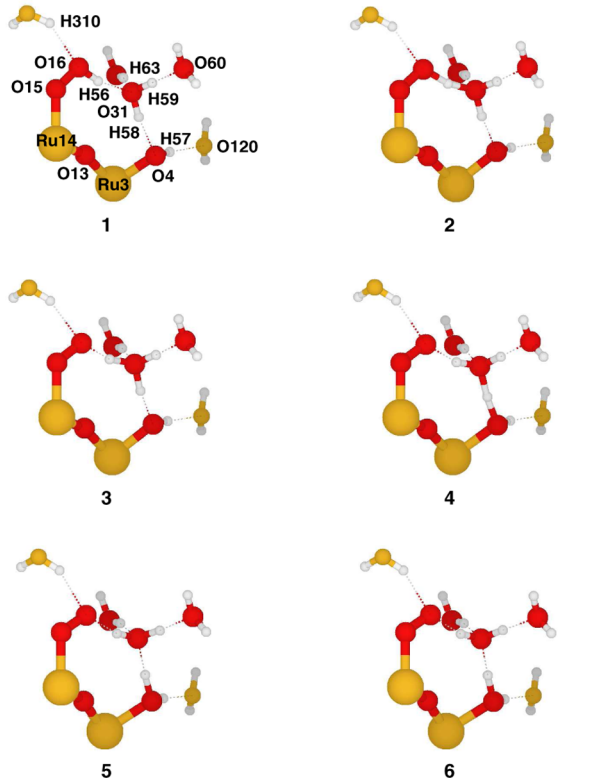

Figure 7. Structures 1−6 along the reaction path in step II as denoted along the bottom axis in Figure 6. In all panels, Ru14 and O15 lie in the plane of the page, while O16 is rotated 35° toward the back of the page. The two waters with the yellow oxygens correspond to classical H_2O's. Structural data are given in Tables 1 and 2.

by the (approximate) equality of the two OH distances in the bonds involved.

4.2.1. From Reactants to PT1. PT1 is identified by structure 2 in Figure 7 and Figure 6b, where the lines of the distances for the proton acceptor O31−H56 (decreasing) and proton donor O16−H56 (increasing) cross. This portion of the reaction path is exothermic by ∼2.3 kcal/mol.

In association with PT1, we register an increase in electron density for O16 and O15 to be left behind by the departing proton and, to a minor degree, for O13 and O4 (cf. Figure 6e), consistent with the transfer of H56 to the PRC water. The increase in electron density on both O13 and O4 signals the beginning of electron flow into the complex and across the μ-oxo bridge, a feature anticipated in Figure 2, II.B.

Another significant change is in the solvation of the PRC water, gauged by lengths of its H-bonds to the neighboring environment. Because this water is accepting a proton, its two hydrogens become more electrophilic, whereas its lone pair not directly involved in PT becomes less basic. These trends are reflected, respectively, in the increase of O31−H63, the decrease of O60−H59 (both in Figure 6c), and the decrease of O4−H58 (cf. Figure 6b). These H-bond changes around the PRC water all assist in the stabilization of the incipient H_3O^+, whose appropriate coordination number is 3 rather than 4.[47−51]

The only noticeable geometric changes in the O15−Ru14−O13−Ru3−O4 unit (Table 2 and Figure 6c) are a mild increase in O13−Ru3 and a decrease in Ru14−O13, respectively. The Ru14−O13, O15−Ru14, and O15−O16 bond lengths are essentially constant throughout the reaction (cf. Table 2) and are omitted from Figure 6c for clarity.

dx.doi.org/10.1021/jp406504h | J. Phys. Chem. B 2013, 117, 15761−15773

Table 1. Structural Parameters along the Energy Profile during the PT Stage of Step II[a]

	O16−H56[b]	O31−H56	O31−H58	O4−H58	O31−H59	O60−H59	O31−H63	H57−O_{120}	O16−H_{310}
1[c]	1.000	1.533	1.012	1.675	1.027	1.541	1.779	1.788	2.038
2	1.218	1.211	1.039	1.541	1.058	1.441	1.860	1.797	2.004
3	1.366	1.105	1.074	1.431	1.076	1.396	1.879	1.785	2.002
4	1.508	1.045	1.196	1.220	1.064	1.420	1.858	1.749	2.020
5	1.627	1.015	1.467	1.054	1.031	1.518	1.767	1.718	1.995
6	1.669	1.011	1.477	1.050	1.030	1.522	1.776	1.722	1.995

[a]Values are shown for bonds in PT region. [b]Atomic labeling is as that in Figure 7. [c]Structure labeling is as that in Figure 6. Distances are in Å.

Table 2. Structural Parameters along the Energy Profile during the PT Stage of Step II[a]

	O15−O16[b]	O15−Ru14	Ru14−O13	O13−Ru3	Ru3−O4
1[c]	1.343	2.077	1.865	2.018	1.968
2	1.334	2.083	1.856	2.038	1.979
3	1.330	2.073	1.855	2.046	1.996
4	1.325	2.057	1.859	1.987	2.071
5	1.322	2.076	1.866	1.955	2.118
6	1.322	2.079	1.862	1.956	2.123

[a]Values shown are for the O−O−Ru═O═Ru−O unit. [b]Atomic labeling is as that in Figure 4. [c]Structure labeling is as that in Figure 6. Distances are in Å.

Table 3. Relevant Atomic Spin Population $\alpha - \beta$ (Löwdin) along the Energy Profile during the PT Stage of Step II

	O16[a]	O15	RU14	O13	RU3	O4
1[b]	0.329	0.580	1.077	0.776	−0.589	−0.186
2	0.433	0.531	1.112	0.746	−0.686	−0.151
3	0.486	0.494	1.142	0.713	−0.735	−0.114
4	0.532	0.463	1.166	0.556	−0.713	−0.024
5	0.577	0.464	1.150	0.444	−0.660	−0.003
6	0.580	0.464	1.162	0.434	−0.674	−0.000

[a]Atomic labeling is as that in Figure 4. The order of the columns reflects the appearance of the atoms from left to right in Figure 4. [b]Structure labeling is as that in Figure 6. Spins are in au.

The $\alpha - \beta$ spin character (cf. Table 3) at the end of this phase is collectively borne by the O15−O16 unit (+0.98), Ru14 (+1.14), O13 (+0.71), and Ru3 (−0.74).

4.2.2. Between PT1 and PT2. This region comprises structures 2, 3, and 4 in Figure 7. The energy drop of ∼1.7 kcal/mol seen in panel a following PT1 involves the generation of the hydronium ion in the PRC and further structural modifications in preparation for the PT2, anticipated in the mechanistic hypothesis in Figure 2.

The full formation of the hydronium ion from the original PRC water in PT1 is signaled by the equivalence of the ion's three bond lengths O31−H56, O31−H58, and O31−H59 slightly past structure 3 in panel b. At this stage, the H-bond length O60−H59 reaches its minimum, andn O31−H63, the length of the H-bond to the weakened lone pair, reaches its maximum (panel c). In preparation of the H58 PT2, the length O4−H58, about equal to O60−H59 at ∼1.4 Å, further decreases. We return to PT2 in a moment.

Between structures 2 and 3, panel e registers the continuous decrease of the charge magnitudes of oxygens O16, O15, O13, and O4, caused by further electron density release to O16 with the completion of PT1 and formation of the hydronium ion discussed above. The values of O13 and O4, in particular, indicate electron flow from O16 across the μ-oxo bridge.

Returning to PT2, its beginning is marked by the increase of O31−H58 between structures 3 and 4 as the proton H58 commences its departure from the hydronium ion. Concomitantly, H-bonding to the hydronium ion starts transitioning to a hydration environment more typical of a water molecule, as indicated by the decrease in O31−H63 and the increase in O60−H59 in Table 1.

In the structures 3−4 interval, we also note the beginning of a change in bond order for Ru3−O4 and O13−Ru3 (panel d), an aspect presented in the mechanistic hypothesis in Figure 2, II.C. In particular, Ru3−O4 loses some double bond character, while electron density is further shifted toward O4, a synergistic feature that will aid PT2 to this oxygen (panel e). This electron density shift away from Ru3 is partially compensated for by the decrease in O13 (panel e) and an increase in the double bond character of O13−Ru3 (panel d). The net effect is an electron density shift from the left-hand side of the complex to its right-hand side, concurrent with PTs also from left to right, increasing the O4 basicity; all of this is illustrated by the resonance structures II.A and II.B in the mechanistic hypothesis in Figure 2.

All of these general trends persist up to PT2 (structure 4), except for changes of the charges on O13 and O15 (panel e), which level out starting with structure 3, and, at this same point, an alteration of the charge on O16, which starts increasing due to the beginning of the dissociation of the hydronium ion.

Table 4. Relevant Atomic Charges (Löwdin) along the Energy Profile during the PT Stage of Step II

	O16[a]	O15	RU14	O13	RU3	O4	O31	H56	H58	H59
1[b]	−0.19	0.00	−0.20	−0.15	−0.27	−0.53	−0.75	0.39	0.40	0.39
2	−0.24	−0.03	−0.19	−0.17	−0.26	−0.55	−0.71	0.42	0.41	0.40
3	−0.26	−0.05	−0.18	−0.18	−0.25	−0.57	−0.69	0.41	0.42	0.41
4	−0.24	−0.05	−0.17	−0.18	−0.25	−0.58	−0.72	0.40	0.43	0.40
5	−0.22	−0.05	−0.17	−0.18	−0.25	−0.56	−0.75	0.39	0.41	0.39
6	−0.23	−0.05	−0.16	−0.18	−0.25	−0.56	−0.75	0.38	0.41	0.39

[a]Atomic labeling is as that in Figure 4. The order of the columns mostly reflects the appearance of the atoms from left to right in Figure 4. The atomic charges for the hydronium ion are given in the last four columns. [b]Structure labeling is as that in Figure 6. Charges are in au.

Table 5. Ligand Mimic Atomic Charges (Löwdin) along the Energy Profile during the PT Stage of Step II

	Q(Ru14,1)[a]	Q(Ru14,2)	Q(Ru3,1)	Q(Ru3,2)	Q(Ru14)	Q(Ru3)	Q_{avg}
1[b]	1.11	1.18	0.99	1.03	1.14	1.01	1.08
2	1.09	1.16	0.99	1.03	1.13	1.01	1.07
3	1.09	1.14	0.99	1.04	1.12	1.02	1.07
4	1.11	1.15	0.99	1.07	1.13	1.03	1.08
5	1.12	1.16	0.98	1.09	1.14	1.04	1.09
6	1.12	1.17	0.98	1.10	1.14	1.04	1.09

[a]Q(Ru14,1) and Q(Ru14,2): total charge on ligands 1 and 2 coordinated to Ru14. Q(Ru3,1) and Q(Ru3,2): total charge on ligands 1 and 2 coordinated to Ru3. Q(Ru14) and Q(Ru3): average charges on ligands coordinated to Ru14 and Ru3, respectively. Q_{avg}: average charge per ligand for the whole complex. Charges are in au. [b]Structure labeling is as that in Figure 6.

4.2.3. From PT2 to Products. This final interval includes structures 4, 5, and 6. It describes the second portion of the final PT from the PRC water center to the Ru−OH hydroxo group, represented by the resonance structure II.C in Figure 2, to produce resonance structure II.D. The energy drop for this interval is ∼3.1 kcal/mol.

Concerning the PRC water, PT2 is already complete by structure 5, as indicated by the constant values of the two components of the PT coordinate, O31−H58 and O4−H58, past this point (panel b). The PT is accompanied by the further weakening of the O16−H56 H-bond due to decreased acidity of H56 following PT2. Concurrently, solvation of the PRC water center, as represented by the decreasing O31−H63 and increasing O60−H59 H-bonds (panel c), returns to resemble that of a neutral water molecule, with a coordination number of 4.

It is interesting to note that, while it is not apparent in the energy profile in Figure 6a, the two PTs in the PRC are stepwise, as is clear from panel b in Figure 6 and the structures in Figure 7.

We also observe (panel d) the final increase of the right-hand side group Ru3−O4 to its value in the PC. Note that the negative charge on O4, the proton-acceptor center, reaches its maximum magnitude at structure 4, at the start of PT2, after which no further electron density increases are necessary.

It is of interest to discuss the nature of the step II PC(II) that we have found. The population analysis of PC(II) (Table 4) indicates a −0.28 e charge on the O2 moiety in Ru−O−O, which is almost entirely assigned to the terminal O, −0.25 e. The spin population difference $\alpha - \beta$ (Table 3) shows a total spin of one unpaired electron, partitioned nearly equally on the terminal O (0.58 spin) and the oxygen bound to Ru (0.46 spin). The O−O bond length is 1.32 Å, similar to the bond length of 1.33 Å in the bare superoxide ion ligand,[52] and the Ru−O distance (2.08 A) is typical for terminal TM superoxide linkages (2.1−2.2 Å).[53] These properties would lead to a Ru(IV)−O_2^- designation in PC(II), the designation that we have used throughout this paper for the product of step II.

However, the aqueous environment should be taken into account to explain the O_2 group's charge and spin polarization. In Figure 7, for the product of step II, structure 6, we find that the terminal oxygen in the Ru−O−O group bears one H-bond (∼1.7 Å) with the water bridging the two end groups, via H56, and another H-bond (∼2.0 Å) to a second, EFP water (H310) that is comparable to the Ru−O bond length (∼2.1 Å). Both of these H-bonds are comparable in strength to the weak Ru−O_2 bond and can shape the electron density of the O_2 moiety.

The two H-bonds just discussed remain in place during the step II relaxation process after PT2 as the reaction ultimately leads to the product PC(II). This illustrates the resilient nature of the cage structure of the water solvent and serves to stabilize the small negative charge on the O_2 moiety, giving it a superoxide character. In an environment in which the H-bonds to the solvent were to weaken, O_2^- could relax to a linkage more closely resembling a neutral O_2 species.

4.3. Charge Populations and Solvation Effects on Step II. Analysis of the charge population along the optimization path (cf. Table 5) show that the 4+ charge of the complex resides essentially on the ligands, +4.3 e, with +2.25 e total on the two organic ligands bound to Ru14 and +2.06 e total on those bound to Ru3, none of which vary appreciably along the reaction path. This may be contrasted with step I,[23] where the average ligand charge from the RC to TS for that step becomes more negative by ∼0.1 e, reflecting an increase in electron density in the complex upon nucleophilic attack by the water molecule. It is worth noting that the apportioning of charge by the Löwdin population analysis yields slightly negatively charged Ru centers and positively charged ligands for this 4+ complex. Similar results were obtained for the step II RC when the bpy ligand was used instead of the model ligand; an average ligand charge of +1.1 was found, and comparable negatively charged values were found for the Ru centers.

The mild variation on the ligand charges in step II is consistent with the small amount of electron density redistribution observed in the O−Ru−O−Ru−O framework during this step, as was shown in Figure 6e. Conversely, in step I, the injection of two electrons into the complex caused most of that extra charge to be temporarily distributed to the ligands.[23] The charge variations just discussed have important consequences for the aqueous solvent effect on reaction barriers, which was large for step I[23] but should be small for step II. We discuss this issue and environmental changes in the catalytic barrier in section 8.

5. REARRANGEMENT PRECEDING STEP II

The starting point for both our mechanistic hypothesis in Figure 2 and the discussion and calculations in the preceding sections for the associated step II has been the reactive complex RC(II), structure II.A in Figure 2 and otherwise denoted as $[HOO(IV,IV)OH]^{4+}$. However, we already pointed out in the introductory remarks in section 2 that our step II does not fully correspond to the reaction in eq 3. In particular, we stressed that this structure is not the product PC(I) of step I for the reaction (structure I.C in Figure 1). As we discussed there, the conformation of PC(I) prevents PT from Ru−OOH to Ru−OH.

In the modeling of step II, we have bypassed the transformation of PC(I) to RC(II) and directly employed structure II.A in Figure 2, which is conducive to a H_2O-mediated PT, in synergy with ET from the Ru−OOH to the

dx.doi.org/10.1021/jp406504h | J. Phys. Chem. B 2013, 117, 15761−15773

Ru−OH across the μ-oxo bridge. Structure II.A is obtainable from structure I.C via the conformational rearrangement displayed in Figure 3, which involves conformational changes within the dimer accompanied by breaking and forming H-bonds with the water solvent. We anticipated in section 2 that this rearrangement, which complements step II to represent the reaction eq 3, would not involve a significant energy cost. Here, we explicitly address this issue.

The construction of a consistent scheme for water oxidation connecting steps I and II is not at all straightforward. The most serious difficulty prevents the straightforward comparison between PC(I) and RC(II) and thus the direct calculation of the energetics for the PC(I) → RC(II) rearrangement from the independently calculated reaction path data of the individual steps I and II. It is that the direct application of the QM/MM cluster method that we have used to describe the nucleophilic attacks and PT reactions in these two steps, which occur with moderate spatial modulation of the surrounding H-bonding subnetwork, would be ill-advised for large-amplitude motions like those involved in the PC(I) → RC(II) rearrangement. The modeling of these large-amplitude motions via straightforward application of our QM/MM cluster method would completely disrupt the H-bonding network of the kind of MRS used in our calculations, just sufficient to provide two solvation shells to the CRS. For a rigorous appraisal, the rearrangement might conceivably be described via ab initio molecular dynamics simulations with periodic boundary conditions, an expensive simulation beyond our present scope.

A much less fundamental issue is the differing numbers of solvating classical waters in the MRSs that we have used for steps I and II, although attention must be paid to key aspects of the solvation. In the step II case (cf. Figure 7, panel 1), the orientation of H57 and its hydrogen bond to O120 required a slightly larger radius for the embedding spherical cluster than the one used in step I in order to ensure that the O120 classical water would be fully H-bonded. For the less important outer echelons of the cluster, small increases in the cluster radius lead to large increases in the number of classical waters. As long as the key solvation requirements described are satisfied and the resulting MRS is tractable with the available computational resources, the number of classical waters is not important, given our ability to link reaction steps with differing numbers of classical waters.

We now elucidate the key features of the rearrangement by two different procedures, which we now present in detail.

5.1. Free-Energy Estimate for the Rearrangement of PC(I) to RC(II). In order to quantify the free-energy change for the rearrangement of the $[HOO(IV,IV)OH]^{4+}\cdot H_2O$ complex from the PC(I) conformation to that of RC(II), calculations were carried out on both assemblies using augmented CRSs embedded in a dielectric continuum.

These augmented CRSs were obtained as follows. By visual examination of the MRSs for PC(I) and RC(II), we first identified key H-bonding interactions in each, which involved the CRS and its complement of solvating classical waters. We then equalized the number of quantum waters for both structures by mutating a few EFPs in each MRS in order to highlight the selected H-bonding interactions. Next, we stripped each modified model system of the classical waters. Finally, we embedded the remaining quantum, augmented CRSs in a dielectric continuum to simulate the aqueous environment for single-point energy calculations. Given the approximate character of this procedure, we neglected any structure reoptimization, including that of the classical waters that were converted to quantum waters.

The resulting augmented CRSs for PC(I) and RC(II) used for the dielectric continuum calculations are shown in Figure 8. The calculated free-energy cost for the rearrangement of PC(I) to RC(II) is 2.7 kcal/mol, a quite modest value.

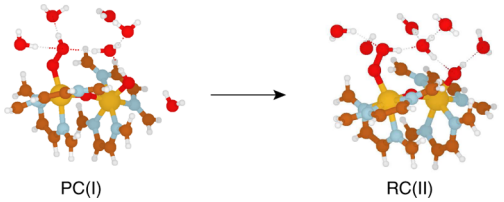

Figure 8. Structures of the augmented CRS of the PC(I) and RC(II) species treated quantum chemically in the dielectric continuum calculations for the free-energy change between these two forms.

In the rearrangement from PC(I) to RC(II) shown in Figure 8, we already see evidence of significant structural changes occurring due to both the conformational changes of the complex and the interactions with the solvating waters. Some of these changes are summarized in Table 6. Most notably, the

Table 6. Summary of Key Bond Lengths for Species in the Rearrangement Phase PC(I) → RC(II) and PT Phase RC(II) → PC(II) of Step II

	O15−O16[a]	O15−Ru14	Ru14−O13	O13−Ru3	Ru3−O4
PC(I)[b]	1.451	1.939	1.937	1.892	1.911
RC(II)	1.343	2.077	1.865	2.018	1.968
PC(II)	1.322	2.079	1.862	1.956	2.123

[a]Atomic labeling is as that in Figure 4. [b]Structure labeling is as that in Figure 6. Distances are in Å.

O15−O16 bond length in the RuOOH group has decreased from 1.451 to 1.343 Å from PC(I) and RC(II) in the rearrangement process of step II along with concurrent increases of 0.138 and 0.057 Å for the Ru14−O15 and Ru3−O4 bond lengths, respectively. This change in the O15−O16 bond length is actually larger than that observed in the PT reactions of step II discussed earlier, where this bond length decreases further to 1.322 Å. Despite these structural changes, as noted above, there is only a small overall free-energy increase (2.7 kcal/mol) involved in the conversion to RC(II). However, this procedure still leaves us without an estimate of any activation barrier for the PC(I) → RC(II) rearrangement, which we now provide.

5.2. Approximate Free-Energy Profile for the PC(I) → RC(II) Rearrangement. We have been able to estimate an upper bound to the activation free energy for the PC(I) → RC(II) rearrangement by calculating the free-energy profile along a partially constrained path for the conformational change between the PC(I) and RC(II) structures.

In order to accomplish this, we have generated a nine-point linear path based on a set of 12 bonding and angular constraints whose limiting values were determined from the structures of the $[HOO(IV,IV)OH]^{4+}\cdot H_2O$ complexes, each in its own conformation, within their corresponding PC(I) and RC(II) MRSs, consistent with Figure 3. The values of the constraints $c_k(x)$ along this linear path are interpolated between the values c_k^0 and c_k^1 corresponding to the structures of PC(I) and RC(II), respectively, as given by the expression

dx.doi.org/10.1021/jp406504h | J. Phys. Chem. B 2013, 117, 15761−15773

Table 7. Values of the Constraints for the 12 Geometrical Parameters Employed in the Constrained Optimizations along the PC(I) → RC(II) Rearrangement Stage of Step II[a]

x	c_1	c_2	c_3	c_4	c_5	c_6	c_7	c_8	c_9	c_{10}	c_{11}	c_{12}
0.000	2.997	2.604	1.937	1.892	168.7	66.8	101.2	6.2	4.0	122.0	97.3	94.7
0.125	2.941	2.607	1.928	1.908	167.7	64.6	89.6	21.9	17.2	107.4	98.1	94.2
0.250	2.884	2.610	1.919	1.923	166.7	62.5	78.0	37.6	30.3	92.8	98.9	93.8
0.375	2.828	2.613	1.910	1.939	165.7	60.3	66.4	53.3	43.5	78.2	99.7	93.3
0.500	2.771	2.617	1.901	1.955	164.6	58.1	54.8	68.9	56.6	63.6	100.4	92.9
0.625	2.715	2.620	1.892	1.971	163.6	56.0	43.1	84.6	69.8	49.1	101.2	92.5
0.750	2.659	2.623	1.883	1.986	162.6	53.8	31.5	100.3	83.0	34.5	102.0	92.0
0.875	2.602	2.626	1.874	2.002	161.6	51.7	19.9	116.0	96.1	19.9	102.8	91.5
1.000	2.546	2.629	1.865	2.018	160.6	49.5	8.3	131.7	109.3	5.3	103.6	91.1

[a]Definition of parameters: c_1: O23−O31, c_2: O15−O31, c_3: O8−Ru9, c_4: Ru7−O8, c_5: ∠Ru7−O8−Ru9, c_6: dihedral ∠O22−Ru9−Ru7−O15, c_7: ∠H57−O23−O31, c_8: ∠H56−O31−O23, c_9: ∠H58−O15−O31, c_{10}: ∠H56−O31−O15, c_{11}: ∠O22−Ru9−O8, c_{12}: ∠O15−Ru7−O8. Bonds are in Å, and angles are in deg. The values of the constraints in PC(I) and RC(II), c_k^0 and c_k^1 in eq 5, correspond to the x = 0 and 1 rows, respectively. See also Figure 9.

$$c_k(x_j) = (c_k^1 - c_k^0)x_j + c_k^0 \qquad k = 1-12 \tag{5}$$

along nine linearly spaced points along the conformational reaction coordinate, x_j, between 0 and 1. The bond and angular constraints c_k are identified in Table 7 and Figure 9. Each

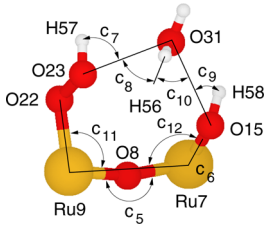

Figure 9. Labeling of the angular constraints used for the calculation of the PC(I) → RC(II) rearrangement. Bond constraints c_1−c_4 are omitted for clarity. All of the constraints are listed in Table 7.

structure along the path is obtained by a gas-phase constrained optimization of the $[HOO(IV,IV)OH]^{4+}\cdot H_2O$ complex. The constrained optimization helps to preserve some memory of the aqueous environments of the PC(I) and RC(II) MRSs while allowing relaxation of the bond lengths in the RuOOH and RuOH groups and of the organic ligand structure. The preservation of a general structure of the complex compatible with the aqueous environment is necessary because the final step in the free-energy profile calculation requires the embedding of the optimized structures in a dielectric continuum.

For consistency along the linear path, we have optimized also the structures at x = 0 and 1 rather than keeping them frozen as in the originating CRSs; failing to do this optimization would result in artificially high energies of these two anchor structures relative to the optimized intermediate structures and would consequently lead to an underestimation of the activation free energy of the rearrangement. All of the optimized structures are displayed in Figure 10.

With these structures, we now need to include solvation effects. These were modeled by embedding the optimized structures in a dielectric continuum of constant ε = 79.8 appropriate for water. The resulting free energetics in water are collected in Table 8 and displayed in Figure 10. The calculated free-energy activation barrier for the PC(I) → RC(II) rearrangement is ∼9 kcal/mol, which should provide a reasonable estimate for this process. The resulting free-energy

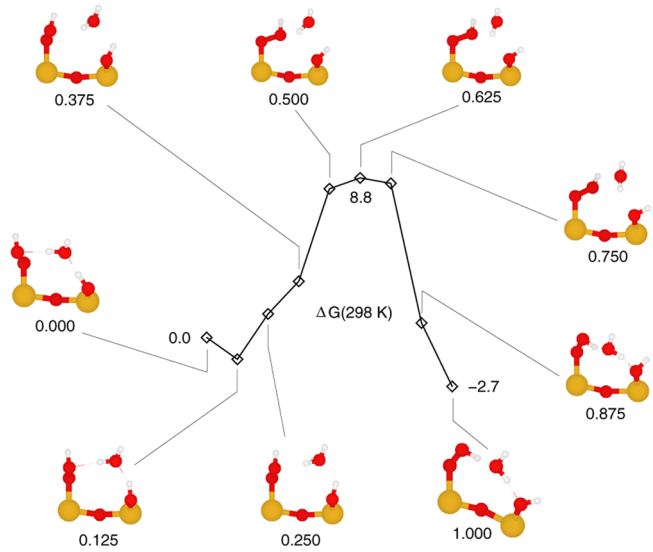

Figure 10. Relative free energies ΔG(298 K) (in kcal/mol) for the intermediate structures in the constrained PC(I) → RC(II) rearrangement of $[HOO(IV,IV)OH]^{4+}\cdot H_2O$. Structures are shown without organic ligands for clarity and are labeled with the x values defined in eq 5 and Table 7.

Table 8. Free Energies of the Intermediates in the PC(I) → RC(II) Rearrangement from the Constrained Optimizations along the Pathway Shown in Figure 10[a]

x	ΔG(298 K)
0.000	0.0
0.125	−1.2
0.250	1.3
0.375	3.1
0.500	8.2
0.625	8.8
0.750	8.5
0.875	0.8
1.000	−2.7

[a]ΔG at 298 K is in kcal/mol. The x = 0 point is chosen as reference. See also Figure 10 and Table 7.

curve, due to the numerous constraints used in the calculations, does not correspond to the optimal conformational path for the rearrangement in aqueous solution; accordingly, our barrier estimate should provide an upper limit.

dx.doi.org/10.1021/jp406504h | J. Phys. Chem. B 2013, 117, 15761−15773

Table 9. Average Charge Per Ligand along the Rearrangement Path PC(I) → RC(II)[a]

	x								
	0.000	0.125	0.250	0.375	0.500	0.625	0.750	0.875	1.000
Q_{avg}	1.069	1.069	1.065	1.057	1.053	1.054	1.057	1.067	1.067
ΔQ_{avg}	0.000	0.000	−0.004	−0.011	−0.016	−0.015	−0.012	−0.002	−0.002

[a]Löwdin charges are in au. ΔQ_{avg} refers to $Q_{avg}(x = 0.000)$. See also Figure 10.

In ref 23, for step I, we had found a correlation between the charge flow into the organic ligands, their interaction with the aqueous solvent, and the contribution of this interaction to the activation free energy. The suggestion in ref 23 was that a hydrophobic environment around the ligands would result in a lowering of the activation free energy. To assess if such a solvent effect is operational also for step II, in the rearrangement phase, we have analyzed the ligands' charge distribution along the rearrangement path in the model system used to calculate the free-energy profile of Figure 10. We find that the average charge per ligand is +1.06 e and +4.24 e for all of the ligands, similar to other steps I and II calculations using a MRS with classical waters instead of a dielectric continuum model. The charges are collected in Table 9. The largest variation of the ligands' average charge over the course of the rearrangement (−0.016 e for $x = 0.5$) is similar in magnitude to the same quantity for the double PT of step II discussed in section 4.3. Consequently, we predict that the reduction of the barrier for step I (eq 2) by a suitable hydrophobic environment will not be accompanied by any significant change in the barrier for the subsequent reaction step II (eq 3). This suggests that eq 3 could become rate-determining in a suitably hydrophobic environment, imposing a limit on the water oxidation rate acceleration by such an environment.

6. WATER OXIDATION SCHEME FOR STEPS I AND II

With the reaction free energy from section 5.1 and the activation free energy estimated in section 5.2, we can now combine the free energetics for steps I and II on a consistent basis to provide a free-energy diagram for the first steps of the water oxidation by the activated $[O(V,V)O]^{4+}$ dimer. The resultant free energies are shown in Figure 11 with important data points collected in Table 10. Here, we discuss how the connections between the separate calculations were made in order to obtain free energies of the species in a consistent manner. Reference to Figures 1−3 can be useful for this discussion.

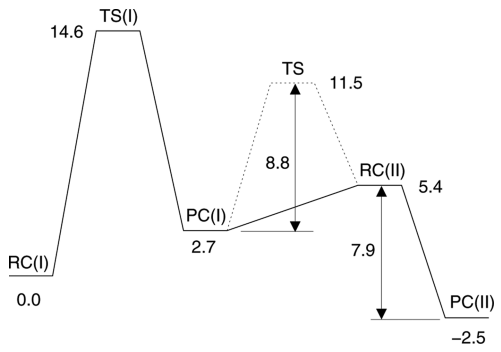

Figure 11. Relative free energies (in kcal/mol) of the combined steps I and II of water oxidation by the Ru dimer $[O(V,V)O]^{4+}$. Shown are the energies for the O−O formation step from RC(I) to PC(I) in step I, the rearrangement process at the beginning of step II from PC(I) to RC(II), and the subsequent PT reactions from RC(II) to PC(II). See also Table 10.

Table 10. Summary of Free Energies of Species for Steps I and II of Water Oxidation by the Ru Dimer $[O(V,V)O]^{4+}$ As Shown in Equations 2 and 3[a]

RC(I)	0
TS(I)	14.6
PC(I)	2.7
TS[PC(I) → RC(II)]	11.5
RC(II)	5.4
PC(II)	−2.5

[a]Free energies are in kcal/mol. See also Figure 11.

For this purpose, it is useful to recall that in the present study, step II is a PRC reaction involving a net PT from Ru−OOH to Ru−OH via a (quantum) H_2O molecule at the center of the chain; that water's presence is consistent with the model of a two-water-molecule PRC chosen for our step I[23] (cf. Figure 1). Furthermore, two additional quantum water molecules were included in the calculations to better describe solvent effects on the central water, while a large number of explicit classical, polarizable waters was used to model the first few solvation shells. In step II, as justified and used for step I,[23] the triplet electronic state was chosen for the modeling.

Step I. The general scheme displayed in the composite free-energy diagram in Figure 11 starts with the reactant of step I, RC(I), which is the fully oxidized Ru dimer, denoted here as $[O(V,V)O]^{4+}$. In the diagram, the free energy of RC(I) is used as the reference. For step I, as O−O bond formation proceeds by attack of a solvent H_2O on one of the Ru═O ends of the dimer, the calculated free-energy activation barrier is 14.6 kcal/mol, while the overall free energy of reaction is 2.7 kcal/mol.[23]

Conformational Transition from the Product of Step I to the Reactant of Step II. Next, Figure 11 employs the connection between steps I and II made by equating the free energies of the step I product PC(I) MRS from ref 23 and that of the PC(I)-augmented CRS embedded in a dielectric continuum of Figure 8. The free energetics of the required PC(I) → RC(II) rearrangement to the RC of step II (cf. Figure 3) were collected from two separate calculations; (i) the free-energy change for the process (cf. Figure 11, solid line connecting PC(I) and RC(II)) was obtained in section 5.1 using water clusters of the TM complex excised from the PC(I) and RC(II) MRSs, whereas (ii) the activation free energy was estimated from a constrained, optimized mapping of the conrotation of the Ru−OOH and Ru−OH groups mediated by a water molecule, all in a dielectric continuum, in section 5.2. This yielded an estimated upper bound for the free-energy barrier of 8.8 kcal/mol and an overall free-energy change of 2.7 kcal/mol.

Step II. Finally, in a process corresponding to the mechanistic hypothesis in Figure 2, when starting from the step II reactant RC(II), two barrierless PTs in a PRC lead to the product PC(II) with a free energy of reaction of −7.9 kcal/

dx.doi.org/10.1021/jp406504h | J. Phys. Chem. B 2013, 117, 15761−15773

mol (section 4). Here, it is worth stressing that RC(II) is not a minimum on the triplet PES because its vibrational frequencies are not all positive. Rather, RC(II), which was initially assembled and partially optimized as a sensible starting structure to locate a minimum, instead spontaneously relaxed to the step II product, PC(II). Lacking the vibrational frequencies for RC(II), we obtained the free energies of both RC(II) and PC(II) by resorting to embedding their respective MRSs in a dielectric continuum.

7. COMPARISON WITH PREVIOUS CALCULATIONS

In ref 23, we have discussed at length the comparison between our step I and the pioneering calculations by Yang and Baik[20] (YB). YB have also examined the analogue of our step II in their study of water oxidation by the Ru dimer, namely, the net PT reaction $[HOO(IV,IV)OH]^{4+} \rightarrow [O_2(III,III)H_2O]^{4+}$. YB considered the reaction as a direct transfer of the proton between the terminal −OOH and −OH groups in the complex without direct chemical involvement of any H_2O molecules. This of course contrasts with the one-water PRC of our step II. (The absence of any explicit waters in YB's model system for step II results from having used a single explicit water molecule in their description of step I; this is in contrast to the two-waters PRC of our step I[23] sketched in Figure 1, which in turn results in a one water PRC in our step II.) Solvent effects were treated by YB using a standard polarizable continuum, equilibrium solvation model, whereas we have used explicit solvating waters, except for the rearrangement calculations of section 5.

YB found step II to have an activation free energy of 5.8 kcal/mol and an overall reaction free energy of −11.2 kcal/mol. The structure of the 2-TS transition state (YB, Figure 4[20]) closely resembles the reactant species with a short RuOO−H bond length (0.98 Å), involving the departing proton, and a much longer O−H separation (2.18 Å) between the proton and the O-acceptor atom on the RuOH end. This TS seems to more closely resemble a conformational change from the product of step I (structure 2 in the YB mechanism[20]) than the traditional three-center intermediate typically encountered in PT processes. Both structures 2 and 2-TS of YB show highly bent Ru−O−Ru bridging angles, 146°, while the present study of step II finds Ru−O−Ru angles of 160−169°. The strain displayed by YB's structures could well be a consequence of the driving force toward formation of a H-bond between the −OOH and −OH groups in competition with the tendency of the Ru═O═Ru unit toward linearity, resulting from the choice of a model system lacking the PRC water present in our model. Thus, the activation barrier may reflect this isolated system choice rather than being representative of the actual PT reaction in aqueous solution.

While YB did not follow the reaction path between the 2-TS transition state and products, they identified, after examining several possibilities, a singlet product $[O_2^-(IV,III)H_2O]^{4+}$ (YB, Figure 5, structure 5[20]) with a free energy of −11.2 kcal/mol relative to the reactant. With an additional H_2O, this species subsequently generates a singlet O_2 complex with the ruthenium dimer (YB structure 6[20]) in a thermodynamically unfavorable process. As an alternative path, YB suggested an intersystem crossing from the singlet to a slightly lower quintet state (structure 5′[20]) with a relative free energy of −20.6 kcal/mol. Such issues did not arise in the present work (and ref 23), where the PES of the triplet state was treated; YB did not report any triplet state structures for step II.

In a recent study, Li, Chen, Schinzel, and Siegbahn (LCSS)[24] examined four complete mechanistic schemes for water oxidation by the blue dimer using a theoretical approach similar to that of YB. In one of these schemes, with its own reference, namely, $[O(V,V)O]^{4+}$ + H_2O, LCSS studied the direct PT step, also with any H_2O molecule directly involved, similarly to YB's treatment. LCSS obtained similar free-energy values for the activation energy (5.1 kcal/mol) and reaction energy (−11.0 kcal/mol) as those obtained by YB.[54] Our reservations concerning the YB treatment also apply to that of this LCSS calculation.

LCSS also considered alternative pathways for water oxidation including predecessors to the $[O(V,V)O]^{4+}$ species as well as direct coupling of the oxo units that are beyond the scope of the present paper. However, one of the mechanistic schemes of LCSS definitely merits further discussion here. The lowest-energy species that occurs in any of the LCSS schemes is the $[HO(V,V)O]^{5+}$ protonated complex, with the proton on one of the oxo groups. LCSS have proposed an alternative and intriguing water oxidation mechanism originating with the protonated species $[HO(V,V)O]^{5+}$. This mechanism departs from the conventional ones that had been developed previously on the basis of experimental evidence[8−11] that presume stepwise oxidation of the $[H_2O(III,III)H_2O]^{4+}$ blue dimer by four equivalents leading to formation of $[O(V,V)O]^{4+}$ as the active species in O−O formation.

However, the only support implicitly offered by LCSS in ref 24 for the existence of $[HO(V,V)O]^{5+}$ is limited to a gas-phase optimization resulting in a stable species. This choice could be considered questionable because, whereas in the gas phase a strongly electrophilic bare proton is likely to bond to the $[O(V,V)O]^{4+}$ complex, in the aqueous phase, a neutral water molecule could successfully compete with the $[O(V,V)O]^{4+}$ cation for the proton, in the view that the acceptor site on the complex, the oxo group, is not as basic as the oxygen in H_2O. This issue deserves further, separate study, starting with the free energetics of formation of the $[HO(V,V)O]^{5+}$ protonated species and its stability in an aqueous environment.

Finally, the issue of possible conformational barriers between conformations of a species as the product of one reaction and the reactant in another is typically not addressed in traditional gas-phase potential energy searches. This contrasts with the present work where the aqueous environment can stabilize different conformers and a noticeable rearrangement barrier was found.

8. CONCLUDING REMARKS

In a previous study[23] of water oxidation by the blue dimer in its activated form, we showed that the initial O−O formation (step I, eq 2), water addition to the $[O(V,V)O]^{4+}$ dimer, occurs by a proton relay chain (PRC) involving two water molecules. In the present work, we showed that in a second step (step II), another PRC involving an intermediary H_2O molecule leads to the reaction in eq 3, $[HOO(IV,IV)OH]^{4+}\cdot H_2O \rightarrow [O_2^-(IV,III)\text{-}H_2O]^{4+}\cdot H_2O$, as displayed in Figure 7 and anticipated in Figure 2. Once an intervening H_2O establishes a PRC between the RuOOH and RuOH termini, the double PT proceeds readily, without activation energy or significant distortions in the TM complex's framework.

This result implies that any activation barrier is not associated with the PT portion of the reaction path but rather with the conformational change necessary to reorient the −OOH and −OH groups from the unreactive conformation of

dx.doi.org/10.1021/jp406504h | J. Phys. Chem. B 2013, 117, 15761−15773

the PC(I) of step I to that conducive to PT in the reactive complex RC(II) for step II. (As stressed in section 2, this means that the reaction in eq 3 consists of this rearrangement and step II).

Accordingly, we have examined an approximate pathway for the rearrangement from PC(I) to RC(II) involving the conrotation of the −OOH and −OH groups in the complex mediated by the water molecule H-bonded to both and kept the model system in the vicinity of this approximate pathway by optimization constraints mimicking the effects of an aqueous solvent cage. This yielded an overall maximum free-energy barrier for the reaction in eq 3 of 8.8 kcal/mol, associated with the rearrangement, and an overall process with a reaction free energy of −5.2 kcal/mol. This result leaves the step I O−O formation in eq 2, with its estimated free-energy barrier of ∼19 kcal/mol,[23] as the rate-determining step for the water oxidation. All of this still leaves unexamined the ultimate step, eq 4, of dioxygen production in the water oxidation; we plan to report on this step presently.

There is a novel aspect in this paper that we believe deserves special attention. It is that intermediates in the solvated phase can have extra processes, for example, PC(I) → RC(II), that are involved in sequential reactions, describing the preparation of the reactant for the next reaction from the product of the preceding reaction, whether the next step happens to be spontaneous (step II) or activated (step III[55]). This strongly contrasts with the standard assumption made in gas-phase calculations for condensed-phase reactions that there is instantaneous transformation from products of one step into reactants of the following step.

We conclude by returning to an issue raised in ref 23. We pointed out there that because charge delocalization in the TM complex's organic ligands during step I is opposed by the surrounding aqueous solvent, a suitable hydrophobic environment, mainly localized around the organic ligands (but still allowing the key participation of water molecules in the PRC), should lower the barrier for O−O bond formation in step I. Should a similar effect be expected for the overall reaction in eq 3 studied in the present work?

In the reactive PRC event, charge redistribution is mostly limited to the PT region and involves only a minimal variation of the organic ligands' charge distribution (section 4.3); therefore, there should not be a significant aqueous solvent effect due to this source. There will of course be some aqueous solvent influence on the PTs in the PRC, but this will not be dramatic so long as a water molecule is included in the PRC. A similarly small charge variation occurs for the rearrangement step preceding the double PT event (section 5.2); therefore, we also anticipate only a minor aqueous solvent influence on its barrier, which is the barrier for the overall reaction in eq 3 studied within.

■ ASSOCIATED CONTENT

Supporting Information

Structures (in Cartesian coordinates) of the model reaction systems along the reaction path, for both the rearrangement (cf. Figure 10) and double proton transfer (cf. Figure 7) portions. This material is available free of charge via the Internet at http://pubs.acs.org.

■ AUTHOR INFORMATION

Corresponding Author

*E-mail: roberto.bianco@colorado.edu.

Notes

The authors declare no competing financial interest.

■ ACKNOWLEDGMENTS

This work was supported in part by NSF Grant CHE-1112564 (J.T.H.) and was also assisted by a seed grant from the University of Colorado Energy Initiative under the Colorado Center for Revolutionary Solar Conversion (CRSP). This work utilized the Janus supercomputer, which is supported by the National Science Foundation (Award Number CNS-0821794) and the University of Colorado Boulder. The Janus supercomputer is a joint effort of the University of Colorado Boulder, the University of Colorado Denver, and the National Center for Atmospheric Research. The calculations were also made possible by access at the National Renewable Energy Laboratory High Performance Computer Cluster, also under the auspices of the Energy Initiative and CRSP. R.B. and J.T.H. are Affiliates of the Renewable and Sustainable Energy Institute (RASEI) at the University of Colorado.

■ REFERENCES

(1) Lewis, N. S.; Nocera, D. G. Powering the Planet: Chemical Challenges in Solar Energy Utilization. *Proc. Natl. Acad. Sci. U.S.A.* **2006**, *103*, 15729−15735.

(2) Lewis, N. S.; Nocera, D. G. Powering the Planet: Chemical Challenges in Solar Energy Utilization. *Proc. Natl. Acad. Sci. U.S.A.* **2007**, *104*, 20142.

(3) Eisenberg, R.; Gray, H. B. Preface on Making Oxygen. *Inorg. Chem.* **2008**, *47*, 1697−1699.

(4) Brimblecombe, R.; Dismukes, G. C.; Swiegers, G. F.; Spiccia, L. Molecular Water-Oxidation Catalysts for Photoelectrochemical Cells. *Dalton Trans.* **2009**, 9374−9384.

(5) Nocera, D. G. Chemistry of Personalized Solar Energy. *Inorg. Chem.* **2009**, *48*, 10001−10017.

(6) Concepcion, J. J.; Jurss, J. W.; Brennaman, M. K.; Hoertz, P. G.; Patrocinio, A. O. T.; Murakami Iha, N. Y.; Templeton, J. L.; Meyer, T. J. Making Oxygen with Ruthenium Complexes. *Acc. Chem. Res.* **2009**, *42*, 1954−1965.

(7) McEvoy, J. P.; Brudvig, G. W. Water-Splitting Chemistry of Photosystem II. *Chem. Rev.* **2006**, *106*, 4455−4483.

(8) Binstead, R. A.; Chronister, C. W.; Ni, J. F.; Hartshorn, C. M.; Meyer, T. J. Mechanism of Water Oxidation by the μ-oxo Dimer $[(bpy)_2(H_2O)Ru(III)-O-Ru(III)(H_2O)(bpy)_2]^{4+}$. *J. Am. Chem. Soc.* **2000**, *122*, 8464−8473.

(9) Yamada, H.; Siems, W. F.; Koike, T.; Hurst, J. K. Mechanisms of Water Oxidation Catalyzed by the *cis,cis*-$[(bpy)_2Ru(OH_2)]_2O^{4+}$ Ion. *J. Am. Chem. Soc.* **2004**, *126*, 9786−9795.

(10) Liu, F.; Concepcion, J. J.; Jurss, J. W.; Cardolaccia, T.; Templeton, J. L.; Meyer, T. J. Mechanisms of Water Oxidation from the Blue Dimer to Photosystem II. *Inorg. Chem.* **2008**, *47*, 1727−1752.

(11) Hurst, J. K.; Cape, J. L.; Clark, A. E.; Das, S.; Qin, C. Mechanisms of Water Oxidation Catalyzed by Ruthenium Diimine Complexes. *Inorg. Chem.* **2008**, *47*, 1753−1764.

(12) Concepcion, J. J.; Jurss, J. W.; Templeton, J. L.; Meyer, T. J. One Site is Enough. Catalytic Water Oxidation by $[Ru(tpy)(bpm)(H_2O)]^{2+}$ and $[Ru(tpy)(bpz)(H_2O)]^{2+}$. *J. Am. Chem. Soc.* **2008**, *130*, 16462−16463.

(13) Sala, X.; Romero, I.; Rodriguez, M.; Escriche, L.; Llobet, A. Molecular Catalysts that Oxidize Water to Dioxygen. *Angew. Chem., Int. Ed.* **2009**, *48*, 2842−2852.

(14) Cape, J. L.; Siems, W. F.; Hurst, J. K. Pathways of Water Oxidation Catalyzed by Ruthenium "Blue Dimers" Characterized by ^{18}O-Isotopic Labeling. *Inorg. Chem.* **2009**, *48*, 8729−8735.

(15) Bernet, L.; Lalrempuia, R.; Ghattas, W.; Mueller-Bunz, H.; Vigara, L.; Llobet, A.; Albrecht, M. Tunable Single-Site Ruthenium Catalysts for Efficient Water Oxidation. *Chem. Commun.* **2011**, *47*, 8058−8060.

(16) Duan, L.; Bozoglian, F.; Mandal, S.; Stewart, B.; Privalov, T.; Llobet, A.; Sun, L. A Molecular Ruthenium Catalyst with Water-Oxidation Activity Comparable to That of Photosystem II. *Nat. Chem.* **2012**, *4*, 418−423.
(17) Chen, J.-F.; Concepcion, J. J.; Meyer, T. J. Rapid Catalytic Water Oxidation by a Single Site, Ru Carbene Catalyst. *Dalton Trans.* **2011**, *40*, 3789−3792.
(18) Maji, S.; Lopez, I.; Bozoglian, F.; Benet-Buchholz, J.; Llobet, A. Mononuclear Ruthenium−Water Oxidation Catalysts: Discerning between Electronic and Hydrogen-Bonding Effects. *Inorg. Chem.* **2013**, *52*, 3591−3593.
(19) Tseng, H.; Zong, R.; Muckerman, J.; Thummel, R. Mononuclear Ruthenium(II) Complexes That Catalyze Water Oxidation. *Inorg. Chem.* **2008**, *47*, 11763−11773.
(20) Yang, X.; Baik, M. H. *cis,cis*-$[(bpy)_2Ru^{V}]_2O^{4+}$ Catalyzes Water Oxidation Formally via In Situ Generation of Radicaloid Ru^{IV}−O·. *J. Am. Chem. Soc.* **2006**, *128*, 7476−7485.
(21) Betley, T. A.; Wu, Q.; Van Voorhis, T.; Nocera, D. G. Electronic Design Criteria for O−O Bond Formation via Metal-Oxo Complexes. *Inorg. Chem.* **2008**, *47*, 1849−1861.
(22) Wang, L. P.; Wu, Q.; Van Voorhis, T. Acid−Base Mechanism for Ruthenium Water Oxidation Catalysts. *Inorg. Chem.* **2010**, *49*, 4543−4553.
(23) Bianco, R.; Hay, P. J.; Hynes, J. T. Theoretical Study of O−O Single Bond Formation in the Oxidation of Water by the Ruthenium Blue Dimer. *J. Phys. Chem. A* **2011**, *115*, 8003−8016.
(24) Li, X.; Chen, G.; Schinzel, S.; Siegbahn, P. A Comparison Between Artificial and Natural Water Oxidation. *Dalton Trans.* **2011**, *40*, 11296−11307.
(25) Ozkanlar, A.; Clark, A. E. Sensitivity of the Properties of Ruthenium "Blue Dimer" to Method, Basis Set, and Continuum Model. *J. Chem. Phys.* **2012**, *136*, 204104.
(26) Hughes, T.; Friesner, R. Systematic Investigation of the Catalytic Cycle of a Single Site Ruthenium Oxygen Evolving Complex Using Density Functional Theory. *J. Phys. Chem. B* **2011**, *115*, 9280−9289.
(27) Lin, X.; Hu, X.; Concepcion, J. J.; Chen, Z.; Liu, S.; Meyer, T. J.; Yang, W. Theoretical Study of Catalytic Mechanism for Single-Site Water Oxidation Process. *Proc. Natl. Acad. Sci. U.S.A.* **2012**, *109*, 15669−15672.
(28) (a) Our approach in ref 23 for step I and in the present work (as well as in the earlier, partial effort referenced below) for step II is consistent with one of the two major experimentally established pathways to O_2 formation in strongly acidic solutions;[8−11] a water molecule from the solvent reacts with a Ru-coordinated oxo group of the catalytically active form $[(bpy)_2(O)Ru^{V}ORu^{V}(O)(bpy)_2]^{4+}$. (b) Bianco, R.; Hay, P. J.; Hynes, J. T. Proton Relay and Electron Flow in the O−O Single Bond Formation in Water Oxidation by the Ruthenium Blue Dimer. *Energy Environ. Sci.* **2012**, *5*, 7741−7746.
(29) Cukier, R. I.; Nocera, D. G. Proton-Coupled Electron Transfer. *Annu. Rev. Phys. Chem.* **1998**, *49*, 337−369.
(30) Huynh, M. H. V.; Meyer, T. J. Proton-Coupled Electron Transfer. *Chem. Rev.* **2007**, *107*, 5004−5064.
(31) Hodgkiss, J. M.; Rosenthal, J.; Nocera, D. The Relation between Hydrogen Atom Transfer and Proton-Coupled Electron Transfer in Model Systems. In *Hydrogen-Transfer Reactions*; Hynes, J., Klinman, J., Limbach, H., Schowen, R., Eds.; Wiley-VCH: Weinheim, Germany, 2007; Vol. 2; Chapter 17, pp 503−562.
(32) Hammes-Schiffer, S. Theory of Proton-Coupled Electron Transfer in Energy Conversion Processes. *Acc. Chem. Res.* **2009**, *42*, 1881−1889.
(33) The classical H_2O effective fragment potential (EFP) employed (see later in the text paragraph) is not suitable for coordination to the hydronium ion H_3O^+ because it promptly accepts a proton and forms the species H_2O−H^+ with an unnatural OH bond with length 0.5 Å.
(34) Hayward, J. A.; Reimers, J. R. Unit Cells for the Simulation of Hexagonal Ice. *J. Chem. Phys.* **1997**, *106*, 1518−1529.
(35) Day, P.; Jensen, J.; Gordon, M.; Webb, S.; Stevens, W.; Krauss, M.; Garmer, D.; Basch, H.; Cohen, D. An Effective Fragment Method for Modeling Solvent Effects in Quantum Mechanical Calculations. *J. Chem. Phys.* **1996**, *105*, 1968−1986.
(36) Chen, W.; Gordon, M. The Effective Fragment Model for Solvation: Internal Rotation in Formamide. *J. Chem. Phys.* **1996**, *105*, 11081−11090.
(37) Becke, A. D. Density-Functional Thermochemistry. 3. The Role of Exact Exchange. *J. Chem. Phys.* **1993**, *98*, 5648−5652.
(38) Stephens, P. J.; Devlin, F. J.; Chabalowski, C. F.; Frisch, M. J. Ab-Initio Calculation of Vibrational Absorption and Circular-Dichroism Spectra using Density-Functional Force-Fields. *J. Phys. Chem.* **1994**, *98*, 11623−11627.
(39) Hertwig, R. H.; Koch, W. On the Parameterization of the Local Correlation Functional. What is Becke-3-LYP? *Chem. Phys. Lett.* **1997**, *268*, 345−351.
(40) Lee, C. T.; Yang, W. T.; Parr, R. G. Development of the Colle−Salvetti Correlation-Energy Formula into a Functional of the Electron-Density. *Phys. Rev. B* **1988**, *37*, 785−789.
(41) Vosko, S. H.; Wilk, L.; Nusair, M. Accurate Spin-Dependent Electron Liquid Correlation Energies for Local Spin-Density Calculations — A Critical Analysis. *Can. J. Phys.* **1980**, *58*, 1200−1211.
(42) Schmidt, M. W.; Baldridge, K. K.; Boatz, J. A.; Elbert, S. T.; Gordon, M. S.; Jensen, J. H.; Koseki, S.; Matsunaga, N.; Nguyen, K. A.; Su, S. J.; Windus, T. L.; Dupuis, M.; Montgomery, J. A. General Atomic and Molecular Electronic-Structure System. *J. Comput. Chem.* **1993**, *14*, 1347−1363.
(43) Stevens, W. J.; Basch, H.; Krauss, M. Compact Effective Potentials and Efficient Shared-Exponent Basis-Sets for the 1st-Row and 2nd-Row Atoms. *J. Chem. Phys.* **1984**, *81*, 6026−6033.
(44) Stevens, W. J.; Krauss, M.; Basch, H.; Jasien, P. G. Relativistic Compact Effective Potentials and Efficient, Shared-Exponent Basis-Sets for the 3rd-Row, 4th-Row, and 5th-Row Atoms. *Can. J. Chem.* **1992**, *70*, 612−630.
(45) Schaftenaar, G.; Noordik, J. H. Molden — A Pre- and Post-processing Program for Molecular and Electronic Structures. *J. Comput.-Aided Mol. Des.* **2000**, *14*, 123−134.
(46) Xfig is an interactive drawing tool that runs under X Window System Version 11 Release 4 (X11R4) or later, on most UNIX-compatible platforms. It is freeware, and available via anonymous ftp at http://xfig.org/userman/.
(47) Ando, K.; Hynes, J. HCl Acid Ionization in Water — A Theoretical Molecular Modeling. *J. Mol. Liq.* **1995**, *64*, 25−37.
(48) Ando, K.; Hynes, J. Molecular Mechanism of HCl Acid Ionization in Water: Ab Initio Potential Energy Surfaces and Monte Carlo Simulations. *J. Phys. Chem. B* **1997**, *101*, 10464−10478.
(49) Ando, K.; Hynes, J. Molecular Mechanism of HF Acid Ionization in Water: An Electronic Structure−Monte Carlo Study. *J. Phys. Chem. A* **1999**, *103*, 10398−10408.
(50) Wang, S.; Bianco, R.; Hynes, J. T. Depth-Dependent Dissociation of Nitric Acid at an Aqueous Surface: Car−Parrinello Molecular Dynamics. *J. Phys. Chem. A* **2009**, *113*, 1295−1307.
(51) Wang, S.; Bianco, R.; Hynes, J. T. Dissociation of Nitric Acid at an Aqueous Surface: Large Amplitude Motions in the Contact Ion Pair to Solvent-Separated Ion Pair Conversion. *Phys. Chem. Chem. Phys.* **2010**, *12*, 8241−8249.
(52) Vaska, L. Dioxygen−Metal Complexes — Toward a Unified View. *Acc. Chem. Res.* **1976**, 175.
(53) Siegbahn, P. E. M. Binding in 2nd-Row Transition-Metal Dioxides, Trioxides, Tetraoxides, Peroxides, and Superoxides. *J. Phys. Chem.* **1993**, 9096−9102.
(54) We ignore here for purposes of argument the fact, stated by LCSS in ref 24, that the structures chosen for the mechanistic scheme might pertain to different electronic states of the reaction system.
(55) Bianco, R.; Hay, P. J.; Hynes, J. T. Theoretical Study of Water Oxidation by the Ruthenium Blue Dimer. III. Mechanism for Oxygen Release in the Step $[bpy_2(O_2^{-})Ru^{IV}ORu^{III}(OH_2)bpy_2]^{4+} + H_2O \rightarrow [bpy_2(H_2O)Ru^{III}ORu^{III}(OH_2)bpy_2]^{4+} + O_2$; To be submitted.